the determination of thermal transport coefficients of various aqueous solutions. Further study should assess the analysis of bad-behaved time-correlation functions of molecular liquids.

Acknowledgement. The authors acknowledge the Korea Research Foundation through Non Directed Research Fund, 1989. The authors thank to the Computer Centers at Kyungsung University for the access to the MV/20000 system and at Pusan National University for the access to the Cyber 803 and Cyber 932.

References

1. C. B. Moon, G. G. Moon, and S. H. Lee, *Bull. Kor. Chem. Soc.*, **12**, 309 (1991).
2. D. J. Evans and G. P. Morris, *Phys. Rev.*, **A30**, 1528 (1984).
3. D. J. Evans and G. P. Morris, *Comput. Phys.*, **1**, 297 (1984).
4. D. J. Evans, W. G. Hoover, B. H. Failor, B. Moran, and A. J. C. Ladd, *Phys. Rev.*, **A28**, 1016 (1983).
5. D. J. Evans, *Phys. Lett.*, **A91**, 457 (1982).
6. D. J. Evans, *Phys. Rev.*, **A34**, 1449 (1986).
7. K. F. Gauss, *J. Reine Angew. Math.*, **IV**, 232 (1829).
8. J. R. Rustad, D. A. Yuen, and F. J. Spera, *J. Chem. Phys.*, **91**, 3662 (1989).
9. (a) F. H. Stillinger and T. A. Weber, *J. Phys. Chem.*, **91**, 4899 (1987); (b) *ibid, Phys. Rev.*, **B31**, 5262 (1985).
10. F. O. Raineri, M. D. Wood, and H. L. Friedman, *J. Chem. Phys.* **92**, 649 (1990).
11. (a) M. S. Green, *J. Chem. Phys.*, **19**, 249 (1951); (b) *ibid*, **20**, 1281 (1952); (c) *ibid* **22**, 398 (1954); (d) R. Kubo, *J. Phys. Soc. Japan* **12**, 570 (1957).
12. G. Ciccotti, G. Jacucci. and I. R. McDonald, *J. Stat. Phys.* **21**, 1 (1979).
13. G. P. Morriss and D. J. Evans, *Molec. Phys.*, **54**, 135 (1985).
14. D. J. Evans, *Molec. Phys.*, **34**, 317 (1977).
15. D. J. Evans and S. Murad, *Molec. Phys.*, **34**, 327 (1977).
16. A. W. Lees and S. F. Edwards, *J. Phys.*, **C5**, 1921 (1972).
17. (a) W. L. Jorgensen, J. Chandrasekhar, J. D. Madura, R. W. Impey and M. L. Klein, *J. Chem. Phys.*, **79**, 926 (1983); (b) W. L. Jorgensen and J. D. Madura, *Molec. Phys.*, **56**, 1381 (1985).
18. (a) G. S. Kell, *J. Chem. Eng. Data* **20**, 97 (1975); (b) N. E. Dorsey, "Properties of Ordinary Water Substances" (Rheinhold, New York, 1940); (c) R. Mills, *J. Phys. Chem.*, **77**, 685 (1974).
19. W. C. Gear, 'Numerical Initial Value Problems in Ordinary Differential Equations' (McGraw-Hill, New York, 1965).
20. S. H. Kuo, "Computer Applications of Numerical Methods" (Addison-Wesley, Philippines, 1972), p. 280.
21. M. Neumann, *J. Chem. Phys.*, **85**, 1567 (1986).
22. S. H. Lee and P. J. Rossky, in "Proceedings of the 10th Korean Scientists and Engineers Conference" (Inchen, Korea 1987), Physical science part, p. 150.
23. W. W. Wood, "Fundamental Problems in Statistical Mechanics III" p. 331 ed. E. G. D. Cohen (1975).
24. S. H. Kuo, "Computer Applications of Numerical Methods" (Addison-Wesley, Philippines, 1972), p. 244.
25. A. D. Simmons and P. T. Cummings, *Chem. Phys. Lett.*, **129**, 92 (1986).
26. (a) P. T. Cummings and G. P. Morris, *J. Phys. F: Met. Phys.*, **17**, 592 (1987); (b) P. T. Cummings and G. P. Morris, *J. Phys. F: Met. Phys.*, **18**, 1439 (1988).
27. B. Y. Wang and P. T. Cummings, *Inter. J. Thermo.*, **10**, 929 (1989).
28. P. T. Cummings and T. L. Varner, *J. Chem. Phys.*, **89**, 6391 (1988).
29. "CRC Handbook of Chemistry and Physics" 70th ed. (CRC Press. Inc., Boca Raton, 1989), F-40.
30. *J. Phys. Chem. Ref. Data*, **15**, 1080 (1986).

Characterization of Spherical Particles by Light Scattering

Sangwook Park, Jungmoon Sung, and Taihyun Chang*

Department of Chemistry, POSTECH, Pohang 790-600
Division of Organic Materials, RIST, Pohang 790-600. *Received January 30, 1991*

We have studied a characterization method of accurate size of spherical particles by fitting experimental light scattering profile to the rigorous theoretical scattering function. An efficient software has been developed for computation of the theoretical scattering function and regression analysis. A light scattering instrument has been built and the necessary data acquisition and analysis are carried out by use of a personal computer with an emphasis on the reduction of analysis and time aiming that this study will be extended toward a development of a practical particle sizing apparatus. The performance of the instrument and the software has been evaluated with latex spheres and found to be satisfactory.

Introduction

Particles exist in various forms, solid (powder), liquid (suspension or emulsion), gas (aerosol), and play an indispensable role in a number of important industrial processes. They exhibit unique properties due to their high surface area to

volume ratio so that their properties are greatly influenced by their size distribution. Therefore more effective particle sizing method has always been in demand and over a few hundred different methods are existent in the literatures. Among these, static light scattering has long been one of the most efficient tools for the characterization of colloidal suspensions.[1-3]

In static light scattering, one measures the time averaged scattered intensity as a function of scattering angle. If the interparticle correlation is absent as in dilute solutions of scatterers, the angular dependence of scattered intensity simply reflects the sum of pairwise interference effects of the scattered optical fields from the scattering centers within an isolated particle.[4] It is called as the particle scattering or structure factor, $S(q)$ and mathematically is equivalent to the spatial Fourier transform of the pair correlation function of scattering centers within a particle, averaged over all possible orientations[5]

$$S(q)=\frac{1}{N^2}<\sum_i^N\sum_j^N \exp\ (i\ q\cdot r_{ij})> \tag{1}$$

where $<\ >$ means the orientational average, N is the number of scattering centers in a particle, r_{ij} the vector connecting two scattering centers, and q the scattering wave vector. The magnitude of q is

$$q=\frac{4\pi n}{\lambda}\sin\ (\theta/2) \tag{2}$$

where n is the refractive index of the medium, λ the wavelength of incident light *in vacuo* and θ is the scattering angle. At low q, the scattering factor is reduced to the well known result[6]

$$S(q)=1\ -\frac{q^2}{3}<R_g^2>+O[q^4<R_g^4>] \tag{3}$$

where $<R_g^2>=\frac{1}{2N^2}<\sum_i\sum_j r_{ij}^2>$ is the mean square radius of gyration. The Zimm plot is one of the famous examples exploiting this feature where one can obtain the radius of gyration from the angular dependence of scattered light intensity.[6] While this method has a distinctive advantage that the particle dimension can be obtained without knowledge of the shape of the particle, it suffers from the restriction that experiments have to be performed at low angle, $qR_g < 1$. For large particles, this condition restricts the experimental validity only at very low angle where reliable measurements are often impractical due to stray light from the strong incident beam.

For some symmetric shapes, however, the particle scattering factor can be analytically obtained in the limit of the Rayleigh-Debey-Gans (RDG) scattering,[7-9] whereby one can determine the dimension of scattering particles by comparing the wide range of observed angular profile of scattered intensity to the calculated one, provided one knows the shape of the particles.[10,11] For example, the particle scattering factor of solid spheres, the shape of interest here, is[7]

$$S(q)=\frac{3}{(qR)^3}\left[\sin(qR)-(qR)\cos(qR)\right]^2 \tag{4}$$

where R is the radius of the spheres.

However, the RDG scattering function fails to describe the scattering from large particles with refractive index significantly different from that of suspending medium. The difference in the refractive indices induces reflection and refraction of the light, which are completely neglected in the simple RDG theory. These phenomena are greatly accentuated either as the particle size becomes larger and/or the difference in refractive indices becomes greater.[12,13] In order to obtain an exact scattering function, it is necessary to solve the electromagnetic equation and its complexity has allowed exact solutions only for a few highly symmetric systems such as spheres[14,15] and oriented cylinders.[13] The rigorous scattering function for solid spheres, usually called as Mie scattering function, is obtained in the form of infinite series and it has not been a trivial job to calculate an accurate function even with the aid of an electronic computer. Therefore a few previous efforts to apply Mie function to a practical particle sizing method have not been very successful.[16-18] Nonetheless, the particle sizing method by Mie scattering is an absolute method which does not require any calibration procedure and the precision of the method can not be compared with other techniques. Also, with the recent rapid progress in microcomputer technology has made the computing power of personal computers powerful enough to calculate the Mie function at a reasonable speed. Therefore the time appears to be mature for the development of a practical particle sizing method using the Mie function. In this study we construct a light scattering instrument and develop a software for a particle sizing method of spheres utilizing the Mie scattering function.

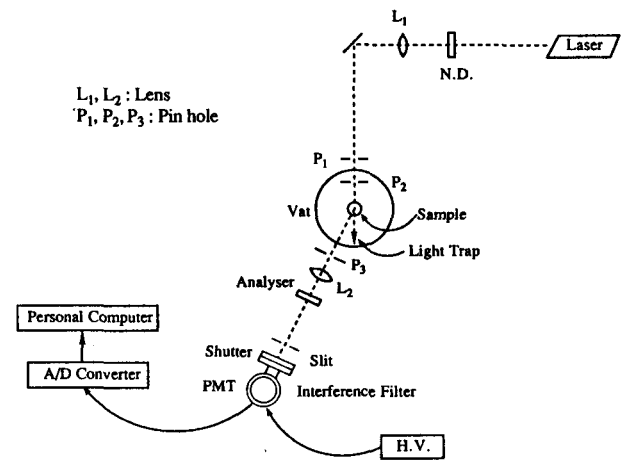

Figure 1. The schematic diagram of the light scattering instrument.

Experimental

The light scattering instrument is built in this laboratory and its schematic diagram is shown in Figure 1. The polarized 632.8 nm line from a He/Ne laser (Spectra-Physics, Model 127-35) is directed to a 10 cm diameter glass vat containing refractive index matching fluid (toluene) and a scattering cell. Its polarization axis is oriented perpendicular to the scattering plane. A 50 cm focal length biconvex lens is used to focus the incident beam at the scattering volume and a pinhole made of light absorbing glass is inserted in front of the scattering cell to reduce the stray light. After passing the cell, the transmitted light is absorbed by a trap,

Table 1. List of Latex Systems and Their Radii Determined by Light Scattering.

Latex	Code	Radius(nm)			
		*	Mie[1]	RDG[2]	SEM[3]
Polystyrene (Polysciences, # 0376)	L-49	49± 1	50± 5		
Polystyrene (Polysciences, # 7304)	L-125	125± 1 (0.124)[4]	135± 2 (0.131)[4]	145± 4 (0.125)[4]	149 (0.137)[4]
Polystyrene (Duke scientific)	L-300	300± 1 (0.297)	297± 2 (0.288)	327± 5 (0.282)	313 (0.288)
Polystyrene (Polysciences, # 7310)	L-510	510± 3 (0.505)	468± 2 (0.455)	533± 8 (0.460)	500 (0.461)
Poly(vinyltoluene) (Duke scientific)	L-1010	1010± 7 (1.000)	1030± 3 (1.000)	1159± 20 (1.000)	1085 (1.000)

*Provided by the suppliers.
[1]Determined by fitting to the Mie scattering function.
[2]Determined by fitting to the RDG scattering function.
[3]Determined by scanning electron microscopy.
[4]Radius/Radius(L-1010)

a piece of light absorbing glass located inside the vat.

The scattered light is allowed to pass through the optical train before reaching a detector. An iris diaphragm controls the angular acceptance of the scattered light and a real image of the scattering volume is projected by a 5 cm focal length lens on the 1 mm width slit which controls the scattering volume. For most of experiments, scattered intensities are strong enough so that the minimum aperture is used which corresponds to the angular acceptance of 1.6°. The scattered light is detected by a photomultiplier tube (Hamamatsu, model R928) and the intensity is recorded by an IBM AT compatible computer *via* an analog to digital converter (Data translation, Model DT2821-F-8DI). The software controlling the data acquisition procedure was written in Turbo Basic (Borland) except the handshaking part between the A/DC board and the PC where an assembler routine was used for fast multiple acquisitions and averaging. Throughout this study, a dichroic polarizer (Melles Griot) was placed before the detector and only the vertically polarized component of scattered intensity was measured.

The program computing Mie scattering function and data fitting was written also in Turbo Basic and the computed Mie functions are found to agree up to 5 significant figures with the most recently published tables[19,20] over all size and refractive index ranges in the table.

A set of standard latex spheres served as a good model system for solid spheres. Dilute aqueous suspensions of latex particles were sonicated for about 10 minutes to disperse the aggregated particles and filtered directly into scattering cells. Glass vials of 21 mm outer diameter with teflon lined caps served as scattering cells. Pore size of the filter (Nuclepore) was typically chosen to be about 3 times bigger than the size of latex particles. After each scattering measurement, the scattering suspension was filtered through a filter whose pore size was less than 1/3 of the latex particles to remove the latex and a scattering experiment was performed on the filtrate in order for background correction. Used latex

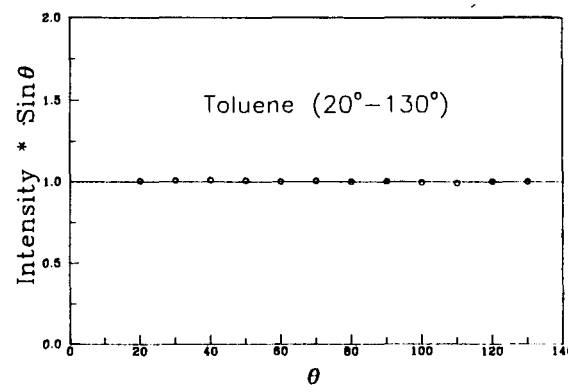

Figure 2. The angular dependence of scattered light from toluene. The intensity is normalized with the scattered intensity at θ=90°.

systems are listed in Table 1 together with the supplier's values of radii which are presumably determined by electron microscopy.

The scattered light intensities, $I(\theta)$ were measured at every degree over the angular range 30° to 140° where the stray light intensity is not too high. After the scan, the extremum positions in terms of the value of sin(θ/2) were determined from $I(\theta)\cdot\sin^4(\theta/2)$ *vs.* sin(θ/2) plot using a software controlled cursor on the video display for later data fitting. Also the size of the latex based on RDG theory can be calculated from the extremum positions easily since $\sin^4(\theta/2)\cdot I(\theta)$ exhibits extrema at the angular position where the following conditions are fulfilled.

$$\tan x=\frac{x}{1-x^2} \quad \text{for maxima} \qquad (5)$$

$$\tan x=x \quad \text{for maxima}$$

where $x=qR$ and R is the radius of the sphere.

Fitting to the Mie scattering function was effected by minimizing the sum of square of residuals of sin(θ/2) value at each extremum position through the regression analysis by using the RDG size as the initial guess. The refractive indices of polystyrene latex, poly (vinyltoluene) latex and suspending medium (water) at the wavelength of 632.8 nm are obtained from the dispersion formulae in the literature[12] as 1.593, 1.577 and 1.332, respectively.

Results and Discussion

The performance of the instrument was checked by measuring angular dependence of scattered light from toluene. The scattered light from small molecules like toluene do not show any angular dependence so that it has been widely used to calibrate the angular dependence of the scattering volume.[1,2] Ideally, our instrumental design should exhibit the angular dependence of scattering volume as $1/\sin(\theta)$[1,2] and it was experimentally confirmed as displayed in Figure 2. The result confirms that the alignment of the instrument is good and the stray light is well controlled in the tested angular range, 20°-130°. Throughout this paper, the scattered intensity, $I(\theta)$ indicates the scattered intensity corrected for the scattering volume by multiplying sin(θ) to the photomultiplier output.

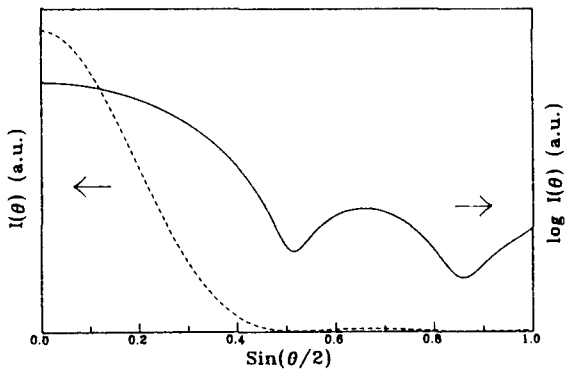

Figure 3. Simulation plots of Mie scattering profiles, $I(\theta)$ and $\log I(\theta)$ *vs.* $\sin(\theta/2)$, for the aqueous suspension of 600 nm diameter polystyrene latex.

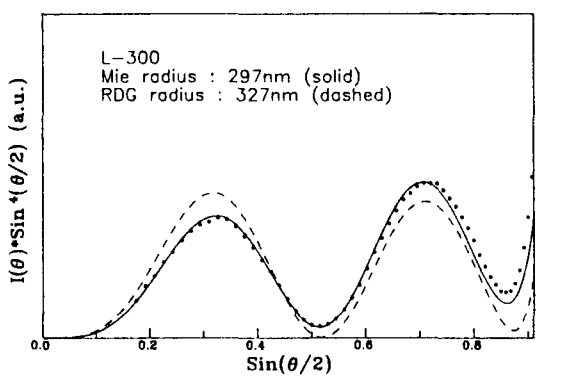

Figure 4. The comparison of RDG theory (dashed line) and Mie theory (solid line) fitting to the experimental scattering profile of L-300 (circles).

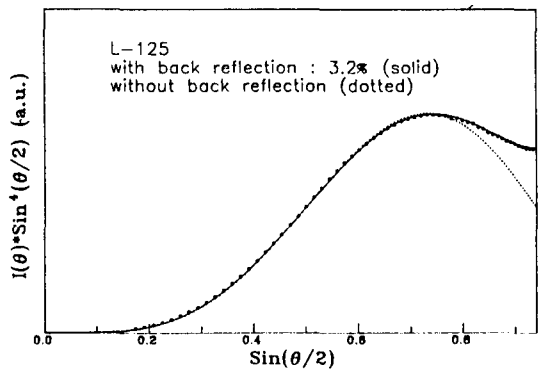

Figure 5. The scattering profile of L-125 (circles) fitted to the Mie scattering profile of 135 nm radius with (solid) and without (dotted) 3.2% back reflection correction.

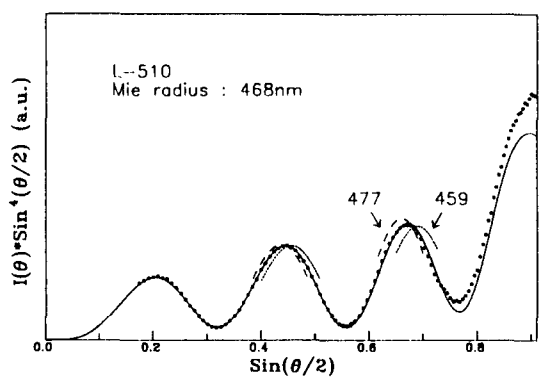

Figure 6. The experimental scattering profile of L-510 and the best fit (468 nm radius) scattering profile determined by Mie scattering function. Two other theoretical profiles for the size with ± 2% deviation in radii from the best fit value (459 and 477 nm) are shown for comparison.

In Figure 3 is shown the Mie scattering simulation profiles of $I(\theta)$ and $\log I(\theta)$ *vs.* $\sin(\theta/2)$, for the aqueous suspension of 600 nm diameter polystyrene latex. While the angular profile of scattered intensity, $I(\theta)$ is rapidly damping with angle, which buries the fine structure of the scattering profile, taking logarithm makes the interference pattern conspicuous. Most of works in this subject so far utilize this type of plots to monitor the interference pattern of the scattering profile. We instead used the plot of $I(\theta)\cdot\sin^4(\theta/2)$ *vs.* $\sin(\theta/2)$ which has more symmetric peak shapes so that the errors in determining the size through extremum position matching procedure can be reduced.[16] In Figure 4 is given an example of such a plot with back reflection correction (see below) for the comparison between RDG and Mie theory. The circles represent the experimental light scattering profile of 600 nm diameter latex suspension (Duke standards). The best fit Mie scattering function (solid curve) with radius of 297 nm is compared to the corresponding RDG scattering function (dashed curve) with 327 nm radius. The computed profiles of both scattering functions were first calculated to best match the angular positions of extrema then rescaled to adjust the amplitude so that they could match the entire profile. First one can notice that the size determined by fitting to the Mie function is in excellent accord with the supplier's value. Ignoring the fact that the size deduced by fitting to the RDG function is off by about 10%, the poor matching of the entire profile indicates that this latex sphere is already too big for RDG theory to be valid.

For this study, it also was necessary to consider that a fraction of the scattered light toward the supplementary angle reflects at the interfaces, where the difference in refractive indices exists, back to the detection optics.[2,21] In this instrument, the interfaces of scattering solution/cell wall and vat wall/air cause such back reflections. Although this contribution can be safely neglected for the systems where the angular dependence of the scattered light is weak such as typical polymer solutions, the large latex particles dealt in this study cause the considerable effect on the scattered intensity at high angles since the scattered light intensity changes orders of magnitude over the experimental angular range for such large particles. The back reflection correction was effected by adding a certain fraction of the scattered intensity at the supplementary angle during the calculation of the theoretical scattering profile and the fraction was chosen empirically to obtain the best fit for all the latex spheres at high angles. The effect of back reflection correction is illustrated in Figure 5 where the light scattering result of the 250 nm diameter latex (Polyscience) is shown. The circles again represent the experimental profile and the solid and dotted lines are the theoretical scattering profile with and without back reflection correction respectively. For the result shown in this figure, 3.2% of the scattered intensity

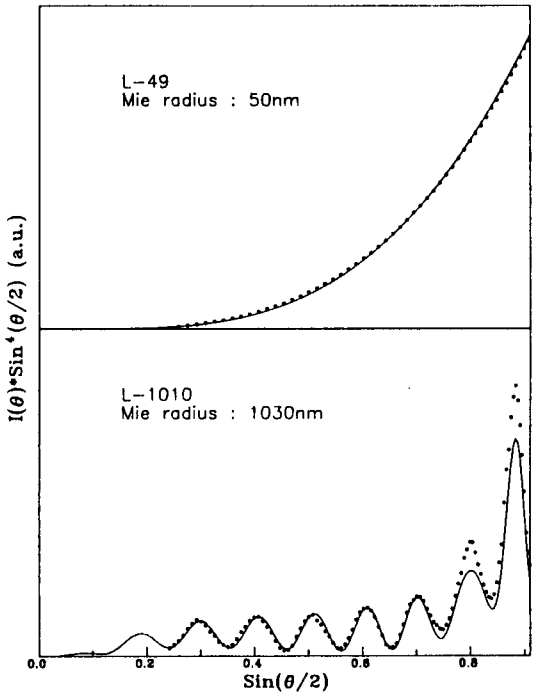

Figure 7. The results of Mie scattering analysis of L-49 and L-1010.

at the supplementary angle is added and the improvement of the fitting is distinct.

Having thus established the general feature of our analysis scheme, the results of scattering data to the Mie functions are shown in Figure 6 and 7 for 3 other latex systems. Considering that only a simple linear rescaling was used for amplitude matching, the quality of matching between experimental profiles to the theoretical ones are remarkable. Furthermore the deduced radii are in excellent accord with those supplied by the manufacturers. In order to demonstrate the precision in fitting the data, two other profiles bracketing the best fit one are shown in Figure 6. Sensitivity of the scattering profile with respect to the radius is apparent, and the precision in the radius determination can be claimed at least 1-2% by this fitting procedure. In Figure 7, we showed the two extreme sizes analyzed in this work, which are apart by more than a order of magnitude. For the smaller size, L-49, the scattering profile does not exhibit an extermum so that we can not claim the precision of the size determination as high as the case of Figure 6. On the other hand, the large L-1010 displays too many extrema and the profile shows the sharp curvature which we suspect to cause the degradation of the fit quality due to the finite angular acceptance of the instrument especially at high angles. However there is no question that we can determine the sizes of them with reasonable precision.

In Figure 8 are shown the scattering profiles at different concentrations of L-510 where the concentration range of the most (a) to the least (c) is about one order of magnitude.

The most concentrated case is the one shown in Figure 6. They demonstrate that the determined radii at different concentrations do not show any trend with concentration, but fluctuate about the mean value at most by 2%. This is because that the length scale of measurements is inversely

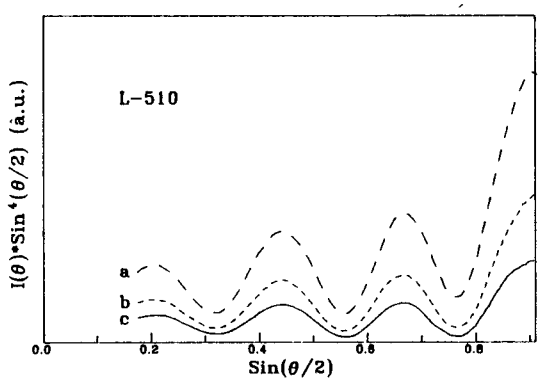

Figure 8. The scattering profiles at 3 different concentrations of L-510 where the concentration range of the the most (a) to the least (c) is about one order of magnitude.

proportional to q which is large at high angle. Therefore the profile at high angle dominantly consists of the contribution from the pair correlation in a short distance apart, *i.e.*, within a particle and the interparticle correlation is only significant at the low angle. This is one of the biggest advantages of the entire profile fitting method over the method which involves extrapolation to zero scattering angle such as Zimm plot where the extrapolation ot zero concentration is also necessary.

All the results from the best fit to both Mie and RDG scattering functions are collected in Table 1. One can easily notice that the results from Mie scattering analyses are in reasonable agreement with the supplier's values except L-510. Considering the sensitivity of our analysis, the deviation found far exceeds the experimental error and it is necessary to measure the size of the latices with an independent method in order to resolve the conflicting results. We selected the scanning electron microscopy for the purpose. Although the accuracy of SEM is suspicious, the reproducibility and precision in determining the size of the latices measured by the same instrument under the same condition are expected. Therefore, electron micrographs of the latices were taken by a scanning electron microscope (Cambridge Instruments, Model Stereoscan 250 Mk 3) at various magnification. The sizes were determined by averaging the size of a number of particles and cross-checked at each magnification. It was found that the sizes at different magnifications were reproducible. Some selected electron micrographs are shown in Figure 9 and determined radii are also collected in Table 1. From the results we can easily notice that the sizes determined with SEM are consistently larger than the light scattering results. Recalling the well known fact that SEM image is apt to exaggerate the size due to edge effects, for fair comparison, the ratios of the size of each latex to the size of L-1010 determined by the respective method of size measurement are given in the parentheses under the radii values. The comparison of these ratios clearly confirms the high accuracy of the Mie scattering analysis in addition to the precision of the method which was demonstrated already.

This procedure can fit experimental scattering function to deduce size in a few minutes which is fast enough to be used as a practical particle sizing method. Hoping that this method will be developed as a practical, high precision particle sizing method, the software developed to compute

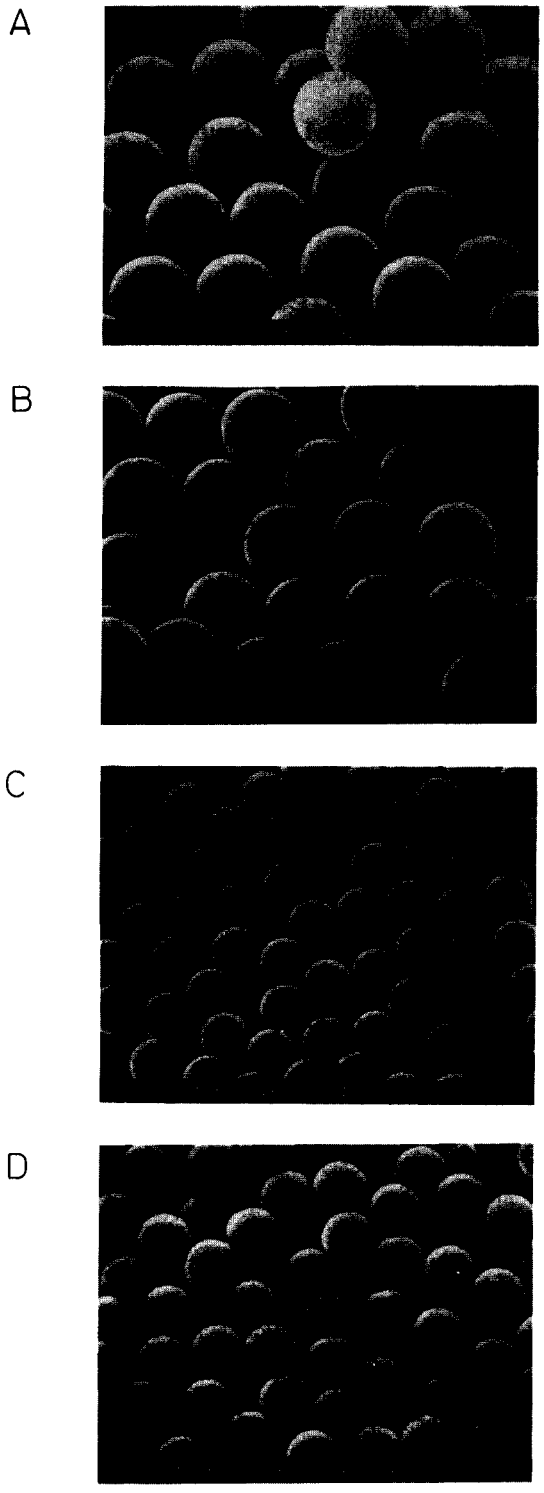

Figure 9. Electron micrographs of latex samples. A: L-1010, B: L-510, C: L-300, D: L-125.

Mie function will be supplied to public upon request. Not only its supreme accuracy shown earlier, the following distinctive features of the light scattering method can be enumerated. First of all, the light scattering is a non-destructive technique with minimal perturbation to the system. Secondly, light scattering probes the internal structure whereas most other techniques monitor the external structure of the particle. Also, it is superior in the sampling statistics which probes about $10^3 \sim 10^6$ particles in this study estimated from the particle number density and the scattering volume.

It would be relevant here to briefly mention the other light scattering technique, dynamic light scattering (DLS), which has become one of the widely used particle sizing methods.[22] In DLS, spectral profile of the scattered light is measured whereby the translational diffusion coefficient of scattering particles is determined. From the diffusion coefficient one can obtain hydrodynamic size of scattering particles. Therefore the principle of the technique differs from that of static light scattering while both techniques make use of the scattered light from the specimen.

In addition to the particle sizing, we can think of other probable applications with this method. Since the simple fitting procedure of the extrema matching reproduce the entire profile as well, a separate nonlinear regression fit of the whole profile was not attempted. Such a fitting can be considered, however, if the information for both refractive index and size of the particle are desired although the rather involved computation is necessary. On the other hand, one may easily obtain refractive index if the size of the latex can be obtained by other means. This would be useful in determining the composition of copolymeric latex. Currently we extend the application of this study to the systems with broad distribution so that not only the average size but the distribution width can also be deduced. This will constitute our next report.

Acknowledgement. This work was supported by grants from the Korea Science and Engineering Foundation. We are grateful to Rrof. Hyuk Yu for his help.

References

1. M. B. Huglin eds. "Light Scattering from Polymer Solutions" Academic Press (1972).
2. P. Kratochvil, "Classical Light Scattering from Polymer Solutions" Elsevier (1987).
3. T. Allen, "Particle Size Measurement, 3rd. Ed." (1981).
4. M. Kurata, "Thermodynamics of Polymer Solutions" Harwood Press (1982).
5. P. Debye, *J. Appl. Phys.*, **15**, 338 (1944).
6. B. H. Zimm, *J. Chem. Phys.*, **16**, 1099 (1948).
7. Lord Rayleigh, *Proc. Roy. Soc.*, **A84**, 25 (1910); **A90**, 219 (1914); **A94**, 296 (1918).
8. R. Gans, *Ann. Phys.*, **65**, 97 (1921); **17**, 353 (1923); **76**, 29 (1925).
9. P. Debye, in "Colloid Chemistry", J. Alexander ed., **1**, 323 Reinhold (1926).
10. V. A. Bloomfield, D. M. Crothers, and I. Tinoco "Physical Chemistry of Nucleic Acids" (1974) Harper and Row.
11. T. Chang, *Polymer (Korea)*, **11**, 195 (1987).
12. M. Keker, "The Scattering of Light and Other Electromagnetic Radiation" Academic Press (1969).
13. H. C. Van de Hulst, "Light Scattering by Small Particles" John Wiley and Sons (1937).
14. G. Mie, *Ann. Physik.*, **25**, 377 (1908).
15. P. Debye, *Ann. Phys.*, **30**, 755 (1909).
16. H. Yu, *J. Res. Nat. Bur. Std.*, **86**(6), 571 (1981).
17. T. P. Wallace and J. P. Kratohvil, *J. Polym. Sci.* **A-2**, 8, 1425 (1970).
18. T. R. Marshall, C. S. Parmenter, and M. Seaver, *J. Col.*

Int. Sci., **55**(3), 624 (1976).
19. W. J. Pangonis and W. Heller, "Angular Scattering Functions for Spherical Particles" Wayne State Univ. Press (1960).
20. H. H. Denman, W. Heller, and W. J. Pangonis, "Angular Scattering Functions for Spheres" Wayne State Univ. Press (1966).
21. S. Bantle, M. Schmidt, and W. Burchard, *Macromolecules*, **15**, 1604-1609 (1982).
22. R. Pecora ed. "Dynamic Light Scattering" Plenum (1985).

Semiempirical MO Calculation of Hetero Atom Three-Membered Ring Compounds (II) · N-Nitroso-azirine and -diaziridine

Ki Woon Hwang

Agency for Defense Development, Taejeon 300-600. *Received February 11, 1991*

Fully optimized MNDO molecular orbital calculations are performed for N-nitroso-azirine (I) and -diaziridine (II). The ground state geometries show the nonplanar configuration around the imino nitrogen. The nitroso group rotational energy barriers and the ring inversion energy barriers are also discussed.

Introduction

Nitrosamines are biologically important cmpounds as cancer suspect agents.[1] Also N-nitrosamines are widely included in many consumer products.[2]

Since three-membered ring compound has large ring strain, three-membered ring with nitrosamine compounds are structually interesting compounds. Structural studies[3-7] of N,N-dimethyl nitrosamine show a planar heavy atom structure. This heavy atom planarity has been explained by partial double bond character between the amino and nitroso nitrogen. Also this partial double bond character inhibits the nitroso group rotation around the N-N bond and makes high nitroso group rotational energy barrier. Previous study[8] showed the ground state conformations, the nitroso group rotational energy barriers and aziridine ring inversion barriers of N-nitroso-aziridine, -oxaziridine, and -dioxaziridine. Here three-membered ring nitrosamine studies were extended to the N-nitroso-azirine (I), and -diaziridine (II).

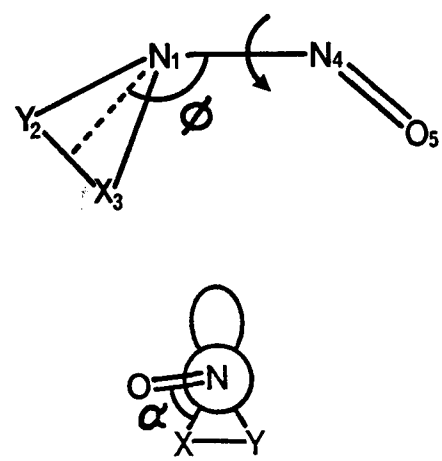

Figure 1. Numbering scheme of atoms and definitions of the angle α and φ: a) X=Y=CH: N-Nitroso-azirine (I). b) X=NH, Y=CH_2: N-Nitroso-diaziridine (II).

Calculation Method

MNDO[9] MO method in the AMPAC[10] program package was used throughout. The AMPAC program was modified for the CDC CYBER 180/860 and run at NOS/VE. All calculations were performed by using standard RHF SCF procedures in the AMPAC. I and II were fully optimized during the calculation to find the ground state conformations. For the transition state of the three-membered ring inversion process, the imino nitrogen was set to planar configuration. Since there are two imino nitrogens in the N-nitroso-diaziridine, N_1 and N_3, two different ring inversion transition states can be calculated. For the energy profile of the nitroso group internal rotation, the nitroso group was set to be eclipsed with the N_1-X_3 bond (see Figure 1) in the three-membered ring and then the nitroso group was rotated counterclockwise 10° increment. In the nitroso group rotational energy barrier calculations, all geometric parameters were allowed to optimize except the nitroso group twisting angle. To find the nitroso group rotational transition state, the nitroso group twisting angle was rotated 1° increment around the energy maximum and finally rotated 0.1° increment. All transition states were confirmed by one and only one negative eigen value in the Hessian matrix.

Results and Discussion

N-Nitroso-azirine (I). The nitroso group rotational energy profile of I is shown in Figure 2. There are two equivalent ground state conformers, B and D. The rotational energy barrier of nitroso group is calculated to be 0.67 kcal/mol. The structure of the rotational transition state of I shows that the nitroso group is eclipsed with the lone pair of the imino nitrogen in the azirine ring, as shown in the previous study.[8] In the ground state of I, the nitroso group is twisted 47.0° from the N_1-C_2 bond in the azirine ring toward the